



Comparison of Pt-BaO/Al₂O₃ and Pt-CeO₂/Al₂O₃ for NO_x storage and reduction: Impact of cycling frequency

Zhiyu Zhou, Michael P. Harold*, Dan Luss

Dept. of Chemical and Biomolecular Engineering, University of Houston, Houston, TX, 77204, United States

ARTICLE INFO

Keywords:

NO_x storage and reduction
Ceria
Platinum
Barium
Oxygen storage capacity

ABSTRACT

NO_x reduction under net lean and near-stoichiometric conditions was carried out on Pt/Al₂O₃, Pt/CeO₂/Al₂O₃ and Pt/BaO/Al₂O₃ washcoated monoliths to compare performance features and identify reaction pathways. The impact of the storage components (BaO, CeO₂) on the NO_x conversion and byproduct (NH₃ and N₂O) yields was quantified for a range of feed temperatures, reductant types (H₂, and C₃H₆), O₂ feed concentrations, and cycle times. The NO_x storage functionality is essential for NO_x reduction under net lean conditions while the oxygen storage functionality promotes NO_x reduction for near-stoichiometric conditions. NO_x conversion by H₂ under lean conditions is dependent on the NO_x storage capacity of the catalyst, with Pt/CeO₂/Al₂O₃ and Pt/BaO/Al₂O₃ exhibiting the highest NO_x conversion below and above 300 °C, respectively. High NO_x conversion is achieved over Pt/CeO₂/Al₂O₃ for anaerobic rich feeds at temperatures above 400 °C. Increasing the O₂ feed concentration enhances NO_x conversion over Pt/CeO₂/Al₂O₃ below 400 °C but inhibits NO_x conversion above 400 °C. The former is attributed to promotion of NO oxidation leading to NO_x storage while the latter is attributed to O₂ inhibition of NO decomposition/reduction. Shorter cycle times increase the NO_x conversion with C₃H₆ as reductant over Pt/BaO/Al₂O₃ under lean conditions and over PCA for the near-stoichiometric feed. The findings confirm that improved NO_x storage utilization is mainly responsible for NO_x conversion enhancement. A ceria redox pathway has only a secondary effect on NO_x conversion under excess O₂.

1. Introduction

Several technologies developed for NO_x abatement are under increasingly stringent regulations [1]. NO_x storage and reduction (NSR) [2] and selective catalytic reduction (SCR) [3] are the most effective but have limitations. Notably, achieving adequate NO_x conversion either at low or high temperatures (< 200 °C or > 450 °C) remains elusive as does the generation and/or release of undesired species such as N₂O and NH₃. NSR [4] involves cycling of lean and rich feeds to the lean NO_x trap (LNT). The rich feed is obtained through modulation of the air-fuel ratio or by fuel injection into the exhaust. The rather narrow temperature window giving high NO_x conversion is ascribed to kinetic limitations at low feed temperature and to NO_x storage capacity, mass-transport limitations and exothermic heat effects at high feed temperatures [4,5]. In contrast, SCR utilizes NH₃ obtained by decomposition of injected aqueous urea for selective reduction of NO_x under net lean conditions. The inadequate NO_x conversion at low (< 200 °C) and high temperatures (> 450 °C) [2,6] is due to constraints of the urea feed system and to the undesired oxidation of ammonia, respectively.

The limitations of NSR and SCR define potential approaches for

improved performance. Several advanced deNO_x techniques or designs have been proposed, such as combination of NSR and SCR [7–9], novel cold start catalysts [10,11], SCR catalyst coated on soot filters, high porous flow substrates [12,13], among others. About 10 years ago Toyota researchers [14] introduced the Di-Air (diesel NO_x after-treatment by adsorbed intermediate reductants) technology, a variant on NSR that involves fast injection of fuel (reductant) into the exhaust upstream of a NSR converter. The Di-Air system is superior to conventional NSR system in many aspects, particularly at high temperatures and space velocities, typically encountered during high load vehicle operation [15].

The enhanced NO_x conversion achieved in the Di-Air system has led to follow-up studies focused on mechanistic investigations and system design and optimization. Zheng et al. [40,41] investigated the enhanced deNO_x performance over a dual-layer LNT + SCR catalyst. Uenishi et al. [42] and Reihani et al. [43] proposed improved designs to minimize axial dispersion upstream of the NSR converter which enabled more intense hydrocarbon pulses. Faster cycling generally has led to higher NO_x conversion with hydrocarbons typically outperforming H₂ or CO at high temperature (e.g. > 350 °C). Both Reihani et al. [18]

* Corresponding author.

E-mail address: mharold@uh.edu (M.P. Harold).

<https://doi.org/10.1016/j.apcatb.2019.05.044>

Received 2 January 2019; Received in revised form 4 May 2019; Accepted 13 May 2019

Available online 14 May 2019

0926-3373/© 2019 Elsevier B.V. All rights reserved.

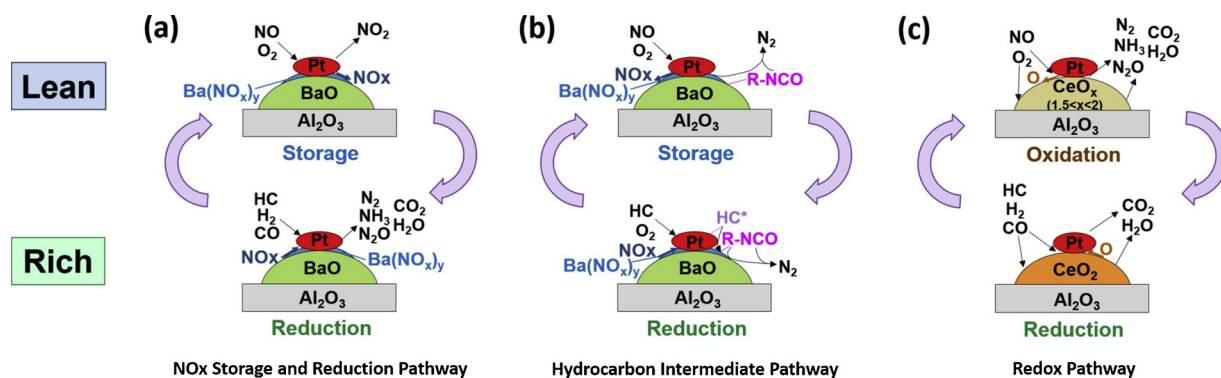


Fig. 1. Three working mechanism possibly involved in the Di-Air system: (a) NOx storage and reduction mechanism; (b) hydrocarbon intermediate mechanism; (c) redox pathway. Here BaO and CeO₂ are chosen to represent the NOx and oxygen storage material respectively.

and Li et al. [19] pointed out that olefins (e.g. C₃H₆ or C₂H₄) are better reductants than the corresponding alkanes. Three mechanisms depicted in Fig. 1 have been proposed to explain the enhanced conversion with fast cycling NSR. These include (a) hydrocarbon intermediates pathway, (b) enhanced NOx storage utilization, and (c) and ceria redox.

The hydrocarbon intermediate pathway (Fig. 1b) proposed [21] by Toyota researchers was based on a combination of reactivity and surface spectroscopy data [14–16]. Isotopic labelling experiments revealed the existence and consumption of thermally stable hydrocarbon intermediates such as nitrous acid esters and amides on the catalyst surface during fast cycling [15]. They concluded that such intermediates, which survive on the surface during fast cycling at elevated temperatures, are subsequently oxidized selectively to N₂. This mechanism was claimed to be mainly responsible for the enhanced NOx abatement performance in the Di-Air system [15].

The conventional NSR pathway (Fig. 1a) with enhanced NOx storage utilization has been proposed and examined in several recent studies [20,22,23]. Reihani et al. [22] compared the dynamic NOx storage capacity at low and fast cycling frequencies and concluded that fast cycling results in more efficient NOx storage and reduction and therefore higher NOx conversion. Ting et al. [20,24] confirmed the presence of hydrocarbon intermediate pathway but ascribed the majority of the enhancement by fast cycling to the conventional NSR mechanism through comparison of the overall deNOx performance with H₂ or C₃H₆ as the reductant. Ting et al. [23] used a non-isothermal 1-D monolith reactor model containing a global kinetic scheme to capture the experimental trends in H₂ case based on the conventional NSR pathway.

The cyclic redox of ceria has been advanced by Makkee and coworkers [25–28,38,74,75]. They used TAP (Temporal Analysis of Products) to show that oxygen vacancies are generated at high temperatures on reduced ceria which serve as sites for NO decomposition/reduction. Ceria has been widely studied since its first application by Ford [29] in 1970s. Due to its unique capability of oxygen incorporation into its crystal lattice [29,30], ceria has been added to supported metal and metal oxide catalysts for enhanced oxidation of emitted reductants, such as the three-way catalyst (TWC) [29], diesel oxidation catalyst (DOC) [31] and diesel particle filters (DPF) [32]. In addition, ceria adsorbs NOx at low temperature, motivating its use in NSR [33–35] and passive NOx adsorption (PNA) [36,37]. Wang et al. [25–28] further showed that carbonaceous species deposited during the pulsing of the reductant (H₂, CO, HC) were converted under the subsequent oxidizing (NO, O₂, CO₂) conditions. While a supported ceria catalyst was effective at high temperatures, the addition of precious metal lowered the temperature needed for the reaction (Pt/CZO and Rh/CZO). Our recent study [39] showed that while NO is effectively converted on reduced ceria at high temperature (> 450 °C), the reduction effectiveness is largely limited due to the competing oxidation by excess O₂ in the feed.

Among the three mechanisms, the conventional NSR pathway and the hydrocarbon intermediates pathway require the participation of adsorbed NOx, accomplished by NOx storage material (e.g. BaO, CeO₂ at low temperature). In contrast, the redox pathway is realized by incorporation of oxygen storage material (e.g. CeO₂).

This study investigates the impact of oxygen and NOx storage materials (CeO₂, BaO) on NOx conversion during fast lean-rich switching. The deNOx performance of three catalysts, Pt/Al₂O₃, Pt/CeO₂/Al₂O₃, Pt/BaO/Al₂O₃, are systematically compared over a range of operating conditions, including cycling frequency, feed temperature, reductant type (H₂, C₃H₆), and oxidant (O₂, CO₂, H₂O) concentrations. The findings are interpreted to advance the understanding and application of fast cycling NSR.

2. Experimental

2.1. Catalyst preparation

Three washcoated monolith samples, Pt/Al₂O₃ (hereafter denoted as “PA”), Pt/CeO₂/Al₂O₃ (“PCA”) and Pt/BaO/Al₂O₃ (“PBA”) were prepared first by synthesizing the powders and then coating small monoliths by slurries containing the active materials. The total washcoat loading was 4.6 g/in³ and the Pt loading was 90 g/ft³. All three catalyst contained ~1 wt. % Pt (washcoat) while the PCA and PBA contained 11 wt. % CeO₂ and BaO, respectively. The powder catalysts were prepared by the incipient wetness impregnation method. The γ-Al₂O₃ (Sasol Inc.) support was calcined in static air at 550 °C for 2 h before impregnation. For PCA or PBA, the γ-Al₂O₃ powder was impregnated with aqueous solution of cerium (III) nitrate hexahydrate (Sigma-Aldrich) or barium nitrate (Sigma-Aldrich), respectively. The powders impregnated with Ce or Ba precursors were dried overnight at 120 °C and calcined in static air at 550 °C for 2 h. The Pt impregnation was achieved by impregnating CeO₂/Al₂O₃, BaO/Al₂O₃ and γ-Al₂O₃ powders with aqueous solution of tetraammineplatinum (III) nitrate hydrate (Sigma-Aldrich). The powders impregnated with Pt precursor were dried overnight at 120 °C and calcined in static air at 550 °C for 2 h.

The Pt/CeO₂/Al₂O₃, Pt/BaO/Al₂O₃ and Pt/Al₂O₃ particles were deposited onto cordierite monolith pieces by a dip-coating method. Blank cordierite monoliths (Mitsubishi, 400 channels per square inch, 1 inch diameter, 2.5 inch in length) were cut into small pieces of (0.42 inch) diameter and (1 inch) length, having ~56 channels. To prepare the PA monolith sample, the PA powder was first ball-milled along with boehmite (AlOOH; Nyacol Nano Technology Inc.) contained in deionized water for 20 h. The monolith piece was immersed from both ends into the Pt/Al₂O₃ slurry for 30 s. Air was then blown for 15 s from both ends of the monolith to remove excess slurry and get a uniform coating. After each round of dip-coating, the monolith was dried at 120 °C for 2 h. Successive dip-coating was applied until the desired

Table 1
Feed gas compositions for cyclic experiments.

Catalyst	BET Surface Area (m ² /g)	Pt Dispersion (%)
PA	119.9	5.3
PBA	99.7	3.4
PCA	112.1	12.4

washcoat loading was achieved (4.6 g/in³). The dip-coated monolith pieces were calcined at 550 °C for 2 h. Monolithic PBA and PCA samples were prepared by a similar dip-coating method, the three monolithic catalysts were aged before reaction evaluation in static air at 700 °C for 33 h, which is equivalent to 160,000 km aging [14].

N₂ physisorption and CO chemisorption tests were conducted to determine the surface area and Pt dispersion for the three samples using a Micromeritics 3 Flex instrument. Catalyst washcoat was scraped from monolith samples for characterization. The results are summarized in Table 1. Physisorption for surface area was carried out using N₂ at 77 K. Chemisorption for Pt dispersion was determined using CO at 35 °C. Physisorption tests show that the three samples (PA, PBA and PCA) had similar. That each of the dispersions is less than 15% is likely a result of the accelerated aging protocol employed. The Pt dispersion for PCA is higher than the values for PA and PBA. This may be due in part to additional CO consumption by reduction of ceria and adsorption on ceria.

SEM was used to determine the thickness of washcoat layer. The thickness of washcoat varied peripherally with a thicker thickness in the corner and a thinner thickness on the wall. The peripherally-averaged thickness for PA, PBA and PCA are 39 μm, 43 μm, 41 μm respectively. Weisz-Prater modulus was calculated to assess the impact of internal diffusion. Detailed discussion was included in Supplementary material (section 7). The washcoat diffusion cannot be isolated in this study but the diffusion impacts in the three samples would be similar, as the three samples has similar washcoat thickness and porosity.

2.2. Bench-scale reactor set-up

A detailed description of the bench-scale flow reactor setup is described in previous studies [40,41]. The feed gas mixture was supplied by a bank of gas cylinders (Matheson Tri-Gas; Praxair, Inc.) and metered by mass flow controllers (MKS Inc.). The gases were fed to the reactor via three different lines: lean line (NO, O₂, Ar), rich line (NO, H₂, C₃H₆, Ar), and main line (CO₂, H₂O, Ar). The main line feed was connected to enable mixing with either the lean or rich line feed upstream of the catalyst. A solenoid-actuated four-way valve (Valco Inc., Micro-electric two position valve) enabled shifting between lean and rich feed at a prescribed switching frequency. A syringe pump (Teledyne Isco model 100DX) and vaporization system were utilized to inject vaporized H₂O into the feed gas. The distance between the injection point and the monolith was ~2 ft in order to reduce the undesired axial mixing (dispersion) of the lean and rich streams, to enable a better comparison to data from previous studies [19,39,40]. The monolithic sample, wrapped by a Fiberfrax® ceramic paper, was placed in a quartz tube (OD = 0.75 in.), contained in a furnace (Thermocraft™). One K-type stainless steel sheathed thermocouple (Omega Engineering Inc.) was placed at the geometric midpoint of the monolithic sample. A FTIR (Thermo Scientific, Nicolet 6700) monitored the concentration of NO, NO₂, N₂O, NH₃, CO, CO₂, C₃H₆ and H₂O. A mass spectrometer (Hiden Analytical, HPR20) monitored the N₂ concentration (m/e = 28). The mass spectrometer was calibrated daily before the start of experiments. When H₂ was used as the reductant and CO₂ was absent in the feed, the N balance was closed within 5%. Otherwise, the amount of N₂ generated was calculated from the overall nitrogen balance because of the overlap of m/e = 28 signal from CO and CO₂ in the mass spectrometer. When C₃H₆ was used as the reductant, the C balance is closed within

Table 2
Feed gas compositions for cyclic experiments.

Run	Rich		Lean		S _N
	Reductant	NO/ ppm	O ₂ /%	NO/ppm	
1	6.21% H ₂	300	5	300	9.7
2	6.21% H ₂	300	0.5	300	1.0
3	6900ppm C ₃ H ₆	300	5	300	9.7
4	6900ppm C ₃ H ₆	300	0.5	300	1.0

5%. When C₃H₆ was the reductant, the N balance cannot be assessed because of the aforementioned m/e = 28 overlap. For both the H₂ and C₃H₆ reductant experiments, H balance and O balance cannot be calculated, as H₂O signal monitored by FTIR is not accurate enough for quantitative evaluation.

2.3. Lean-rich cyclic experiments

Lean-rich cycling experiments were conducted over the three monolithic catalysts (PA, PCA and PBA). The data for the PBA and PCA samples are compared to PA to assess the contribution of the BaO and CeO₂, respectively. Two reductants (H₂ and C₃H₆) tested the overall NOx abatement performance obtained by the three catalysts. The total system flowrate was 3000 sccm, corresponding to a gas hourly space velocity (GHSV) of 76,000 h⁻¹ (at STP). Table 2 summarizes the feed conditions used in the cyclic experiments. The lean to rich time ratio was 6 to 1 (14.3% rich duty cycle). The fixed duty cycle set the fuel to oxidant ratio. The lean/rich frequencies used in the study spanned 90 s/15 s, 60 s/10 s, 30 s/5 s and 6 s/1 s. The cycle-averaged stoichiometric number was used to characterize feed stoichiometry by

$$S_N = \frac{[NO] + 2[O_2]}{[H_2] + 9[C_3H_6]} \quad (1)$$

The O₂ concentration was varied to provide a cycle-averaged stoichiometric feed, either (S_N = 1.0) or lean feed (i.e. S_N = 9.7). In some experiments the O₂ concentration was varied to study its impact on the deNOx performance (i.e. S_N varying from 0.03 to 9.7). In most experiments, CO₂ and H₂O were excluded to minimize the impact from side reactions (i.e. water gas shift reaction and competitive adsorption on BaO or CeO₂ sites). CO₂ and H₂O were added in several experiments to study the impact of CO₂ and H₂O.

The cyclic experiments were carried out at feed temperatures ranging from 150 °C to 600 °C with 50 °C temperature increments. Before each set of experiments, the catalyst was pretreated in 2% H₂ until NH₃ was not detected in the effluent, then by 2% O₂ for 10 min, and finally by a 10 min Ar purge. This procedure ensured that no stored NOx accumulated and that the catalysts were fully oxidized. Once a cyclic stationary-state was reached, results from up to 10 cycles were averaged to determine the cycle-averaged reactant (NOx and C₃H₆) conversion and product (N₂O and NH₃) yield. The cycle-averaged reactant (NOx and C₃H₆) conversions (X_{NOx}, X_{C₃H₆}) and NH₃ and N₂O yields (Y_{NH₃}, Y_{N₂O}) were calculated by standard expressions reported in the Supplementary Material.

In the current study our experimental approach was to turn off the O₂ during the rich injection in order to avoid the steep exotherm [17,20]. For example, Ting et al. [20] reported temperature rise of up to 300 °C during propylene injection into an O₂-containing feed, under net rich conditions. This approach enables a clearer performance comparison of the Pt/BaO/Al₂O₃ and Pt/CeO₂/Al₂O₃ catalysts, which is the main objective of this study. In one of the first Di-Air reports by Toyota researchers, Inoue et al. [14] showed that high NOx conversion may be achieved through rapid reductant injection into a simulated lean exhaust stream while maintaining an overall lean condition throughout the cycle. However, other researchers reported that high NOx conversion could only be achieved with a net rich rapid pulse [17,19,20,43].

In our studies, enhanced NO_x conversion could be achieved with a net rich pulse.

2.4. NO_x storage experiments

The NO_x storage capacities of each of the three samples (PA, PCA and PBA) were measured under a continuous feed of 300 ppm NO and 5% O₂. Prior to each NO_x storage experiment, the catalyst was fully regenerated by applying the pretreatment procedure described above. The NO_x storage capacity, C_{NO_x} , is calculated from

$$C_{NO_x} = \frac{F_{NO_x} t^* - \int_0^{t^*} F_{NO_x}(t) dt}{m_{wc}} \quad (1)$$

where t^* is the duration and m_{wc} the washcoat mass.

2.5. Steady-state experiments

Selected steady-state experiments were carried out to determine the impact of mixing over the PCA sample using feeds with various S_N values. In all steady-state experiments, the feed temperature was 550 °C and contained 300 ppm NO, 8891 ppm H₂, varied concentration of O₂ and balance Ar. The S_N was varied between 0.5 and 1.5 through variation of the O₂ concentration. The PCA sample was pretreated following the procedure described in 2.3.

3. Results

3.1. Impact of catalyst formulation

In this section, we compare the overall NO_x abatement performance over each of the catalysts for a cycle-averaged lean feed ($S_N = 9.7$) conducted at the fastest cycling frequency (6/1 s) and using with H₂ and C₃H₆ as reductants. H₂O or CO₂ were excluded in these experiments to avoid interference from side reactions. The impacts of H₂O and CO₂ are primarily discussed in the Supplementary Material (section 6) [20].

Fig. 2 compares the cycle-averaged NO_x conversion for the three catalysts as a function of feed temperature with either H₂ (2.a) or C₃H₆ (2.b) reductant. For both H₂ and C₃H₆, PA is inferior to PBA and PCA over the entire temperature range. This confirms the promotional impact of BaO in storing NO_x and of CeO₂ in storing O₂ and NO_x. For H₂, the NO_x conversion using PA or PCA decreases monotonically with feed temperature while for PBA the conversion exhibits a local maximum at ~300 °C. PCA outperforms PBA in the lower temperature range ($T < 300$ °C) while PBA outperforms PCA for intermediate and high temperatures ($T > 300$ °C). For C₃H₆, the NO_x conversion obtained with both PBA and PCA exhibits a local maximum at an intermediate temperature; specifically ~50% at ~400 °C for PCA, and ~65% at ~450 °C for PBA. In contrast, the NO_x conversion obtained with PA is below 10% over the entire feed temperature range. The NO_x conversion for PCA slightly exceeds that for PBA for feed temperatures below 400 °C while PBA significantly outperforms PCA at higher temperatures. These trends are consistent with those reported by Yang et al. [41] who showed that the addition of ceria to Pt/BaO/Al₂O₃ promotes cycle-averaged NO_x conversion over a wide intermediate temperature range (175 °C–400 °C). The promotional impact diminishes at high temperatures (~4% at 400 °C). The specific differences in the NO_x conversions for the three catalysts can be largely explained by their discrepant NO_x storage capacities. We return to this point below.

Fig. 2.c shows the cycle-averaged C₃H₆ conversion over each of the three catalysts as a function of feed temperature. (Note: The H₂ conversion in the H₂ experiments is not reported as the H₂ was not measured.) For each catalyst the C₃H₆ conversion remains low (< 15%) for temperatures below 300 °C. The merging of the conversions in this range is reflective of the equal Pt loading (1 wt.%). Upon light-off, the C₃H₆ conversion rank is PCA > PBA > PA. Propylene consumption

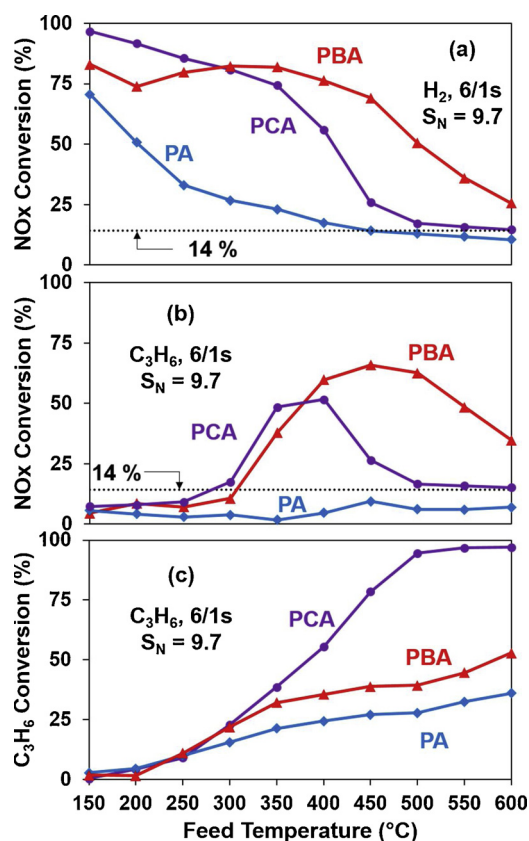


Fig. 2. Cycle-averaged reactant (NO_x and C₃H₆) conversions as a function of feed temperature. [Conditions: lean/rich switching frequency: 6/1 s; lean: 300 ppm NO, 5% O₂, balance Ar; rich: 300 ppm NO, 6.21% H₂ or 0.69% C₃H₆, balance Ar, tested catalyst: PA, PCA, PBA].

occurs through its catalytic reaction with O₂ due in part to unavoidable upstream mixing between the rich and lean feeds. With its limited capacity to store NO_x or O₂ in this temperature range, catalytic oxidation by gaseous O₂ is the primary C₃H₆ conversion pathway. Consumption also occurs through reaction of C₃H₆ with stored NO_x and/or stored oxygen. The increased conversion obtained for PBA vs. PA is probably due to its reaction with stored NO_x. The much larger incremental increase for PCA is clearly a result of its reaction with oxygen stored by the ceria [29,30].

Fig. 3 shows the estimated amount of stored NO_x on the three samples as a function of feed temperature. These were estimated from NO_x effluent profiles by the method described in the Supplementary Material (Fig. S1). Previous NSR studies [23,44,69] show that NO_x storage involves at least three sequential steps. In the first step complete NO_x storage occurs, evidenced by the absence of NO or NO₂ in the effluent. The second step, commences at NO and/or NO₂ breakthrough,

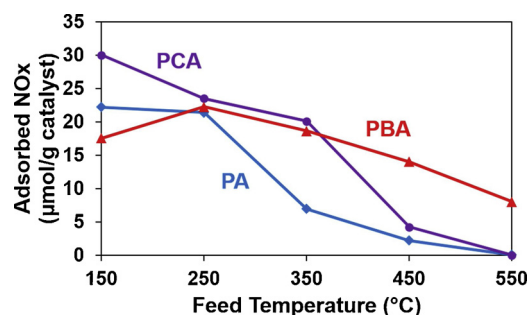


Fig. 3. Calculated amount of adsorbed NO_x on PA, PCA or PBA as a function of feed temperature. [Conditions: 300 ppm NO, 5% O₂, balance Ar].

involves an increasing effluent concentration of both species, and lasts for 10's of seconds. The third step is the much slower approach of the NOx concentration to its feed level and may last for several minutes to hours. Since the current study focuses on NOx abatement performance over a range of cycle times, the time period of interest is confined to 60 s. For temperatures below 350 °C PCA has a slightly higher NOx storage than PBA and PA. At temperatures exceeding 400 °C, PBA outperforms both PCA and PA. Even at temperatures as high as 550 °C PBA retains some NOx storage capacity while both PCA and PA have none. These data are consistent with previous works [33–35]. Bulk barium nitrate and nitrite species decompose in air at 590 °C and 267 °C, respectively [4]. In contrast, the NOx storage contributed by CeO₂ [33–35] and Al₂O₃ [45,46] occurs at much lower temperatures. Ji et al. [35] reported that surface nitrates formed on Pt/CeO₂ remained stable at 300 °C but disappeared upon heating to 400 °C. Al₂O₃ may also contribute to the NOx adsorption at temperatures below 300 °C [45]. These results are under “dry” conditions – NOx storage on PA is much lower in the presence of H₂O. Nitrates and nitrites formed on Al₂O₃ with a co-feed of NO and O₂ but those are weakly bound and displaced by H₂O [72]. Nitrates and nitrites [4] formed on CeO₂ or BaO surface still survive with H₂O introduction, as CeO₂ and BaO possess relatively stronger basicity compared to Al₂O₃.

A comparison between the cycle-averaged NOx conversion and NOx storage provides insight into the working mechanism. With H₂ as reductant, the impact of catalyst composition on cycle-averaged NOx conversion (Fig. 2.a) follows the trends of the short-time NOx storage data (Fig. 3) with two exceptions described below. For temperatures < 300 °C, PCA has the highest NOx storage capacity (Fig. 3) and the highest NOx conversion (Fig. 2.a). In contrast, at higher temperatures (> 400 °C), PBA exhibits the highest NOx storage (Fig. 3) and as a result outperforms PCA and PA during fast cycling (Fig. 2.a). Two exceptions to the connection between storage and conversion are encountered at 150 °C and 350 °C. At 150 °C, PBA has a higher NOx conversion but a lower NOx storage than PA. This may be explained by the difference in the stability of nitrates or nitrites on PBA and PA. That is, nitrate species formed on Al₂O₃ can be easily purged in an inert gas at the same temperature [45] while nitrate species formed on BaO remain stable during inert purging [4]. Thus, even though PA traps more NOx during the lean feed, the loosely held NOx desorbs from the surface, preventing its reduction. At 350 °C, PCA has a lower cycle-averaged NOx conversion but has a slightly higher NOx storage compared to PBA. This contradiction may be explained by the oxygen storage of PCA. Ren et al. [33] pointed out that on a ceria-containing NSR catalyst, the reductant reacts with both stored NOx and oxygen. Thus, in cyclic experiments with PCA, additional consumption of reductants may result in a lower reductant concentration and a lower cycle-averaged NOx conversion.

For C₃H₆ as reductant, the dependence of cycle-averaged NOx conversion (Fig. 2.b) also follows the fast NOx storage trends at temperatures exceeding the propylene light-off (e.g. > 300 °C). With C₃H₆ as reductant PCA outperforms PBA over a wider range of temperature than with H₂; i.e., up to ~350 °C. The promotional effect of ceria is through mitigation of the self-inhibited propylene oxidation on Pt. Previous NSR studies have shown that hydrocarbons are inferior to H₂ due to self-inhibition [47,48]. Lang et al. [31] showed that the addition of ceria, albeit with Pd/Al₂O₃, lowers the light-off temperature of C₃H₆. In summary, the consistent dependence of cycle-averaged NOx conversion on the fast NOx storage capacity validates the importance of the conventional NSR mechanism at higher cycling frequency.

Figs. 2.a and 2.b show that PCA outperforms PA over the entire feed temperature range with both H₂ and C₃H₆ as reductant. However, the difference diminishes at higher temperatures (> 400 °C). In fact, the NOx conversion approaches ~14% for both PCA and PA at feed temperatures exceeding 500 °C. This value in fact corresponds to the fraction of the cycle that is rich; i.e., 1/7, showing that the NOx reduction only occurs during the rich part of the cycle at high temperature. The

only slightly higher NOx conversion on PCA compared to PA, i.e., 4% higher for H₂ and 8% for C₃H₆, suggests that the benefits of CeO₂ under lean conditions (S_N = 9.7) is limited. In our previous study [39] we reported that the rate of NO decomposition/reduction over PGM-free ceria is greatly diminished due to the higher reactivity with oxygen vacancies of O₂ compared to NO. In the current study using Pt/CeO₂/Al₂O₃, the NOx conversion is almost certainly confined to the rich phase when there is a large excess of O₂. These results suggest that ceria has only a limited promotional impact on the deNOx under fast cycling conditions. These conclusions are not likely to be much different if O₂ is present during the reductant injection. On the other hand, there is a sustained enhancement in the NOx conversion on PBA compared to PA at high temperature. Figs. 2.a and 2.b show a NOx conversion enhancement at 600 °C of ~15% and ~28% for H₂ and C₃H₆, respectively.

The performance with Pt/CeO₂/Al₂O₃ and Pt/BaO/Al₂O₃ confirm a decidedly minor role of oxygen storage material (CeO₂) while underscoring the critical role of NOx storage material (BaO). These findings agree with those of Reihani et al. [43] who reported that the fractional NOx conversion achieved with a Pd-Rh TWC under fast cycling was only slightly higher than 15%, the percentage of rich time among the total lean-rich cycling time for a 15% duty cycle. They attributed the inferior deNOx performance to two factors; the low NOx storage due to lack of NOx storage material, and the inferior NO oxidation due to the absence of Pt.

Figs. 4.a and .b recast the cycle-averaged NOx conversion data for PBA and PCA, respectively, to more clearly show the impact of the reductant type. At low to intermediate temperature (< 400 °C), H₂ is the superior reductant for both PBA and PCA. This finding is consistent with previously-reported results and is attributed to the much lower light-off temperature of H₂ on Pt-containing catalyst [49]. At high temperature (> 450 °C) there is no longer an advantage of H₂. In fact, to the contrary, the NOx conversion with C₃H₆ slightly exceeds by ~10% that obtained with H₂ on the PBA catalyst (Fig. 4a). The NOx conversion enhancement with C₃H₆ under fast cycling has been previously reported [16,18–20]. Earlier studies attributed the enhancement to the formation of a thermally stable hydrocarbon surface intermediate that is selectively oxidized to N₂ during the lean part of the cycle [16,24]. Most recently Ting et al. [71] show via modeling of experimental results that the advantage of C₃H₆ is a result of its lower external mass

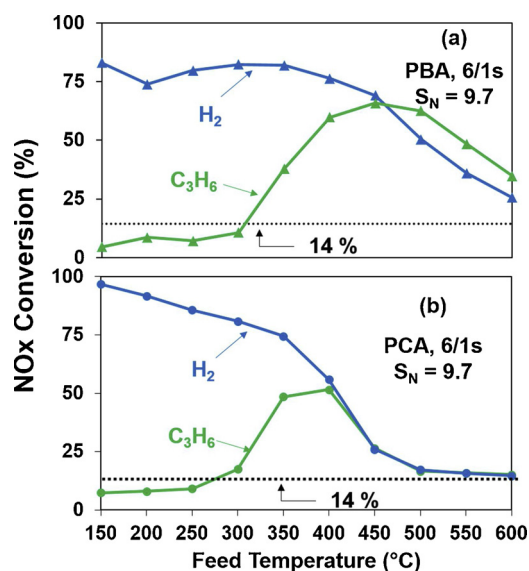


Fig. 4. Comparison of cycle-averaged NOx conversion as a function of feed temperature over PCA or PBA with H₂ or C₃H₆ as the sole reductant. [Conditions: lean/rich switching frequency: 6/1 s; lean: 300 ppm NO, 5% O₂, balance Ar; rich: 300 ppm NO, 6.21% H₂ or 0.69% C₃H₆, balance Ar; tested catalyst: (a) PBA; (b) PCA].

transfer rate compared to H_2 and the resulting lower release of NO during the rich pulse. On PCA both H_2 and C_3H_6 give essentially the same 14% NOx conversion (Fig. 4b) indicating that reduction only occurs during the rich feed. Earlier discussion pointed out that the redox pathway has only a minor contribution to the NOx reduction performance under net lean conditions ($S_N = 9.7$). For the PCA catalyst, the nearly identical NOx conversion of ~14% above 450 °C for both H_2 and C_3H_6 suggests that any additional reduction on the ceria is negligible. We expand on the redox mechanism on ceria in the next section. Results of NH_3 and N_2O yields over three catalysts with H_2 or C_3H_6 as sole reductant are reported in the Supplementary Material (Section 2) [51–55].

3.2. Role of CeO_2

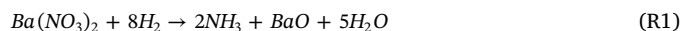
As introduced earlier, the enhanced NOx conversion observed during fast cycling at high temperatures, is attributed to one of three mechanisms; (1) improved NOx storage utilization, (2) adsorbed hydrocarbon intermediate pathway, or (3) ceria redox pathway. The low NOx conversion obtained during lean-rich cycling on Pt/ CeO_2 compared to Pt/BaO suggests that the redox pathway is secondary. To investigate this further, we compare the overall and transient NOx abatement behavior over the PCA catalyst for various cycling frequencies and feed conditions. Similar to the last set of experiments, H_2O or CO_2 were excluded from the feed to avoid complications from side reactions (e.g., water gas shift reaction) in order to isolate the impact of CeO_2 .

3.2.1. Impact of O_2

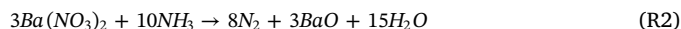
Fig. 5 describes for PCA the cycle-averaged NOx conversion (5.a, b), NH_3 yield (5.c, d) and N_2O yield (5.e, f) as functions of feed temperature for cycle time ratios spanning 90/15 s to 6/1 s and for two feed compositions, $S_N = 9.7$ (Figs. 5.a, c, e) and $S_N = 1.0$ (Figs. 5.b, d, f). For comparison, results and discussion on the impact of cycling frequency over Pt/BaO/ Al_2O_3 (PBA) are included in Supplementary Material (Section 3) [4,20,23,73]. The NOx conversion increases with decreasing cycle time over the entire feed temperature range for both lean and stoichiometric feeds. For the lean feed ($S_N = 9.7$), the beneficial impact of fast cycling diminishes at temperatures > 500 °C which, is a result of less effective NO decomposition in the presence of excess O_2 . Hence NO is only reduced during the rich part of the cycle. In contrast, for the stoichiometric feed ($S_N = 1$) the NOx conversion approaches a plateau that incrementally expands beyond 14% with decreasing cycle time. For example, $X_{NOx} \sim 34\%$ for the 6/1 cycle. The conversion increase with decreasing cycle time at lower temperatures is a result of the improved NOx storage utilization on the ceria. It is noteworthy that the lean feed gives a higher conversion than the stoichiometric feed. This is

attributed to the higher yield of NO_2 from Pt-catalyzed NO oxidation, which is of positive order in O_2 . Crocoll et al. [64] studied the NO oxidation over Pt/ Al_2O_3 catalyst under oxygen excess conditions. It was found that the increase in the O_2 concentration from 1.5 vol.% to 6.0 vol.% led to a monotonic increase of NO conversion to NO_2 over a wide temperature range (150 °C–500 °C). The PCA NOx storage capacity results for the $S_N = 1.0$ and $S_N = 9.7$ cases are shown in Fig. S3 (Supplementary Material). The results show that a higher O_2 feed concentration gives a higher NOx storage capacity on PCA when PCA still possesses NOx storage capacity (i.e. < 450 °C). In this case, the increased NO oxidation from the O_2 concentration increase results in an enhanced NOx storage, which in turn gives a higher NOx conversion under net rich conditions.

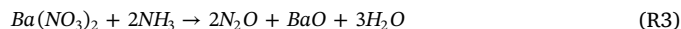
Fig. 5c and d show that the cycle-averaged NH_3 yield is a non-monotonic function of temperature for both feeds at all cycle times. The maximum NH_3 yield occurs at an intermediate temperature (250 °C–400 °C) and is slightly skewed to lower values for the lean feed. To the right of the maximum the yield approaches ~14%, indicating all the NO that reacts is converted to NH_3 under these conditions. The lone exception is the 6/1 cycle with the lean feed for which the yield limit is ~10%. For temperatures sufficiently left of the yield maximum, an increase in the cycle time decreases monotonically the NH_3 yield. This trend conveys that a more efficient oxidation accompanies the faster cycling. Previous NSR studies of Pt/BaO/ Al_2O_3 have shown that during regeneration, NH_3 is generated upstream from the reaction of H_2 with stored NOx in reaction R1:



The NH_3 subsequently reacts with stored NOx downstream oxidized by NO and O_2 to N_2 by reaction R2 [50,51]:



N_2O may also form via reaction R3 [73]:



Lietti et al. [56] identified the different temperature thresholds for the two steps on a Pt/BaO/ Al_2O_3 catalyst and concluded that NH_3 formation (R1) is faster than NH_3 consumption (R2). This should increase the net formation of NH_3 (R1). Indeed, an increasing dependence of NH_3 yield with cycle frequency was observed in Pt/BaO/ Al_2O_3 case as shown in Fig. S2 (Supplementary Material). In contrast, with its oxygen storage capacity, PCA promotes NH_3 oxidation (R2) which decreases the net generation of NH_3 . The decrease in NH_3 yield with shorter cycle time is attributed to enhanced oxidation reaction of NH_3 . NH_3 formation occurs in the front part of the monolith during the rich H_2 pulse; the faster cycling increases the contact of the rich and lean feeds which results in the enhanced extent of reaction. This trend is

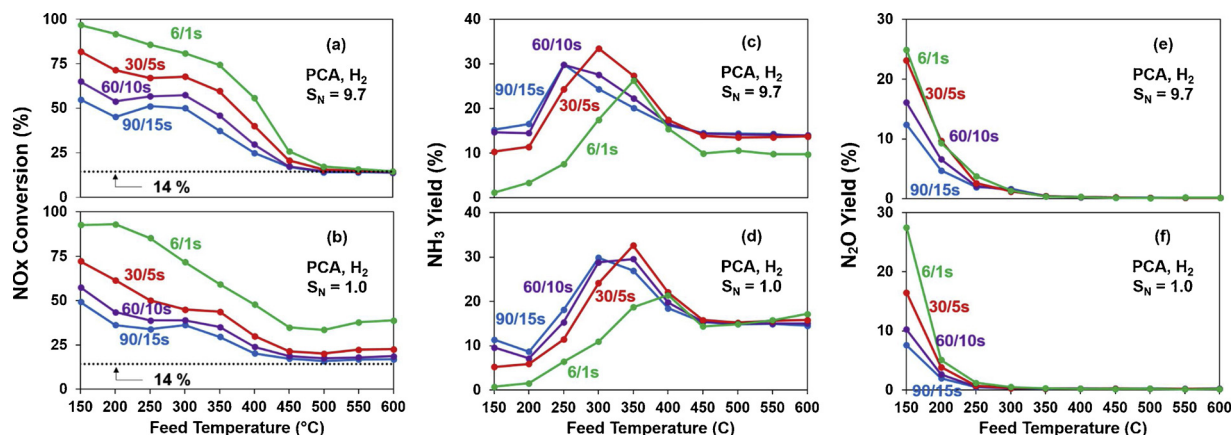


Fig. 5. Cycle-averaged NOx conversion, NH_3 yield and N_2O yield over PCA as a function of feed temperature. [Conditions: lean/rich switching frequency: 90/15 s, 60/10 s, 30/5 s, 6/1 s; lean: 300 ppm NO, 5% O_2 ($S_N = 9.7$) or 0.5% O_2 ($S_N = 1.0$), balance Ar; rich: 300 ppm NO, 6.21% H_2 , balance Ar].

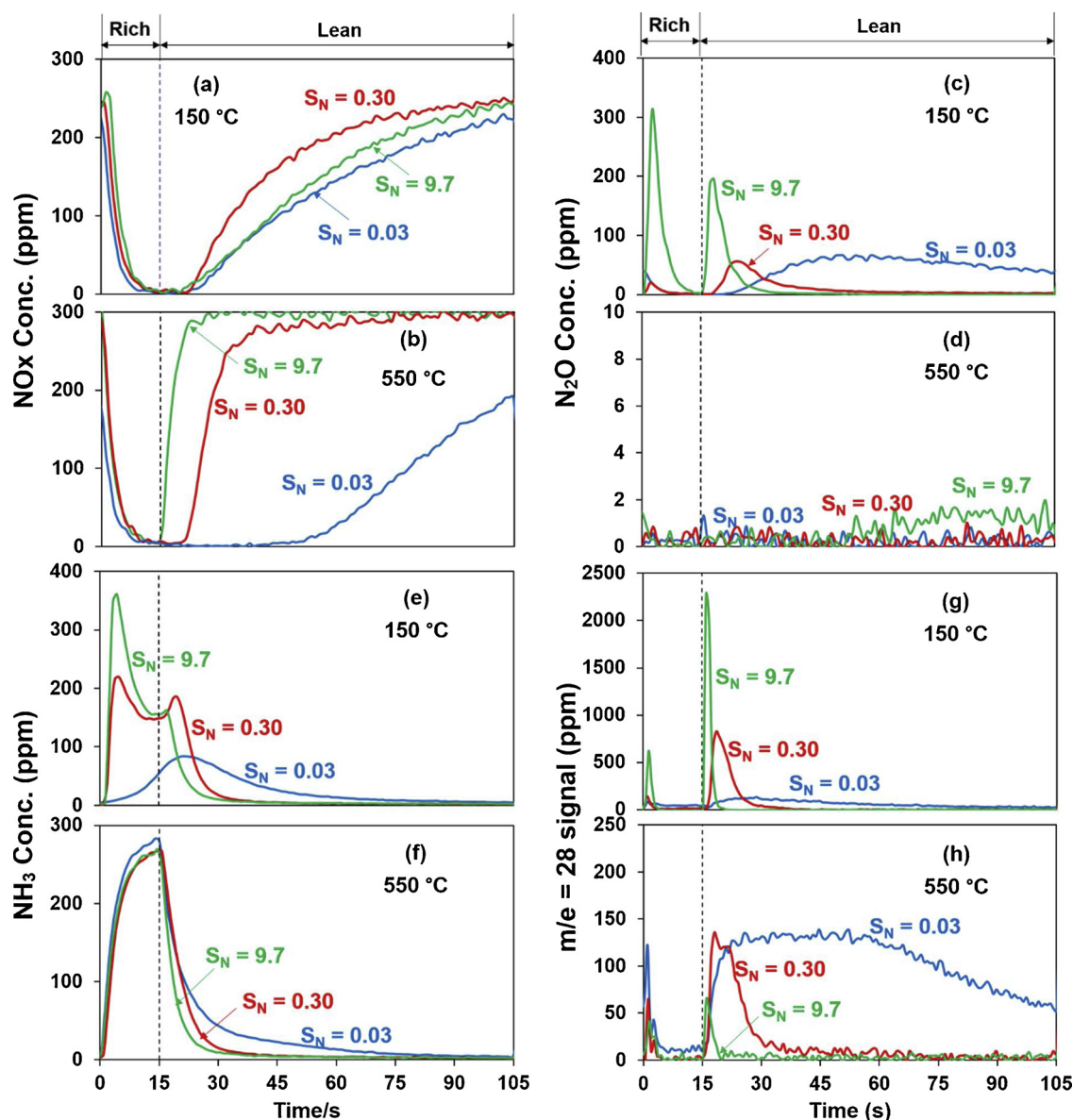


Fig. 6. Effluent Concentration profiles for a set of cycling experiments with PCA using varied O_2 concentration. [Conditions: lean/rich switching frequency: 90/15 s; lean: 300 ppm NO, no O_2 ($S_N = 0.03$) or 1400 ppm O_2 ($S_N = 0.30$) or 5% O_2 ($S_N = 9.7$), balance Ar; rich: 300 ppm NO, 6.21% H_2 , balance Ar; feed temperature: 150 °C or 550 °C].

consistent with Ting et al. [23] who used a NSR catalyst containing a higher loading of PGM (Pt + Rh) and mixture of BaO and CeO_2 . We did not include the quantitative analysis here. It is not feasible to carry out a quantitative analysis under fast cycling (e.g. 6 s lean/1 s rich) due to the FTIR gas cell mixing. The highlighted global reactions follow from the analysis of previous studies [23,51,56,66,73].

Fig. 5.e and .f show that for both feeds, the N_2O formation only occurs at low temperatures (e.g. < 300 °C) and its yield increases monotonically with decreasing cycle time for a fixed temperature. N_2O formation on PCA results from two paths; the first is a reaction between NO and reductant or surface-deposited reductive species over reduced PGM sites via the NSR pathway, while the second is reaction of NO over partially reduced ceria via the redox pathway. A shorter cycle leads to the faster oxidation/reduction transition of PGM sites and ceria, both of which promote N_2O formation and result in a higher N_2O yield.

The NOx and O_2 storage functionalities and their contributions to NOx reduction may be assessed by examining the transient species concentrations at 150 °C and 550 °C. Effluent transient profiles of nitrogen-containing species provide a more detailed look at the

underlying chemistry during the lean-rich cycle (Fig. 6). The ceria NOx storage capacity decreases to a negligible value for temperatures above 400 °C [35] while the oxygen storage is sustained at high temperatures on activated ceria (i.e. > 150 °C for H_2) [57]. PCA exhibits oxygen storage function at both 150 °C and 550 °C but has NOx storage function only below 450 °C. Therefore, the deNOx performance at 550 °C presents the sole contribution from redox pathway. Ting et al. [23] pointed out that mixing inside the FTIR gas cell results in a protracted tail for ~20 s in this experimental setup at the given flowrate. To suppress the interference from the tail, we focus on analysis of the transient data from the longest cycling time 90/15 s. The mass spectrometer (MS) signal of $m/e = 28$ includes contributions from both N_2 and N_2O [58] when H_2 is the reductant and the feed is devoid of CO_2 . The N_2 part of the $m/e = 28$ signal may be adjusted by subtracting the N_2O FTIR measured contribution. The FTIR mixing effect prevents a complete deconvolution of the N_2O and N_2 contributions from the $m/e = 28$ signal.

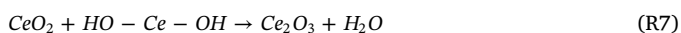
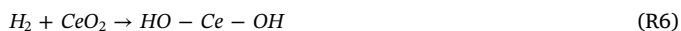
To better understand the impact of O_2 on NOx reduction performance over PCA, a set of experiments was conducted with varied O_2

concentration in the lean feed for a 90/15 cycle at feed temperatures of 150 °C and 550 °C. Three lean feeds having different O₂ concentrations (0, 1400 ppm, 5%) were applied having the following respective values of S_N: 0.03, 0.30 and S_N = 9.7. The results of these experiments are shown in Fig. 6; i.e. NOx (Fig. 6.a and b), N₂O (Fig. 6.c and d), NH₃ (Fig. 6.e and f), and m/e = 28 (Fig. 6.g and h). The m/e = 28 signal intensity was converted to N₂ concentration using a N₂ calibration factor. Following earlier comments, the N₂ concentration is estimated by comparing transient plots of m/e = 28 signal and transient plots of N₂O (i.e. subtracting N₂O contribution from the overall m/e = 28 signal). Considering the limited formation of N₂O at 150 and 550 °C, Fig. 6g and h are good estimates of the N₂, notwithstanding the slower dynamics of the N₂O FTIR signal.

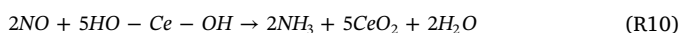
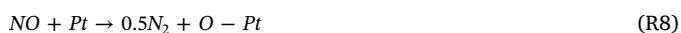
The rich cycling feed (S_N = 0.03) serves as a reference in that no O₂ is contained in the feeds. The NOx profile exhibits a similar pattern at 150 °C (Fig. 6a) and 550 °C (Fig. 6b) despite the widely different temperatures. After a quick decrease during the rich feed, the NOx remains undetected for ~10 s and ~30 s at 150 and 550 °C, respectively. Following breakthrough, the NOx slowly increases to its feed value. At both temperatures N₂ exhibits a continuous generation throughout the entire lean feed along with an additional small peak evident at the start of the rich feed. The protracted NH₃ tail during the lean feed exceeds the ~20 s tail produced by the FTIR cell, suggesting that NH₃ is generated throughout the lean period. The reduction of NO and generation of NH₃ in rich involves the reaction of NO with adsorbed H during the rich feed; i.e.,



Also, the reduction of ceria or PGM-containing ceria by H₂ leads to the formation of vacancies (R5) [29,30,62] and H adatoms (R6, R7) [39], which may be utilized for NO reduction in lean period.



Reactions R8 - R10 describe NO reduction to N₂ and NH₃ over reduced Pt-CeO₂ during the lean period:



The similar NOx, N₂ and NH₃ effluent profiles indicates the existence of the redox pathway.

The impact of O₂ on NOx reduction at high temperature (i.e. 550 °C) is discussed first due to its comparative simplicity. Previous studies [25,28] pointed out that O₂ is a better oxidant than NO to re-oxidize ceria or Pt/CeO₂. Correspondingly, our study shows that the addition of O₂ has an inhibitory impact on NOx conversion. Fig. 6.b shows that the addition of O₂ to the lean feed leads to a large increase in unreacted NOx such as an earlier and sharper slip of NOx. For the S_N = 9.7 feed, NOx slips and reaches the feed level (300 ppm) almost immediately upon the switch from rich to lean feed. This suggests that NOx reduction only occurs during the rich feed and beginning of the lean feed. Accordingly, the addition of O₂ strongly inhibits N₂ formation during both the lean and rich feeds. This results in a smaller N₂ peak during the rich feed and a diminished N₂ formation period during the lean feed (Fig. 6.h). For example, for the first peak N₂ ~ 50 ppm and disappears after ~ 2 s. At 550 °C, NH₃ is mainly formed during the rich period with limited additional generation during the lean period. In comparison, for the S_N = 0.03 case, NH₃ has a large formation during the rich and as mentioned above is sustained for ~ 60 s into the lean period (Fig. 6.f). Similar to N₂, the addition of O₂ decreases NH₃ generation during both the lean and rich feeds. The detrimental impact of O₂ on NOx conversion at 550 °C is attributed to the competition between NO and O₂ for

surface vacancies and hydroxyls.

At 150 °C the NOx reduction data reveal classical NOx storage and reduction behavior (Fig. 6.a) [33,34]. For each of the feeds, the NOx decays quickly upon the switch from lean to rich and remains undetected in the remaining part of rich feed. This trend is consistent with H₂ reduction of co-fed NO and NOx trapped on the ceria phase during the lean period. NOx remains undetected for ~5 s in the beginning of lean feed and then increases towards the feed concentration. The lean NOx slip is a nonmonotonic function of the O₂ concentration.

Previous studies [33–35] suggest that Pt/CeO₂/Al₂O₃ exhibits considerable NOx storage capacity under net lean conditions at medium and low temperatures (< 400 °C). Haneda et al. [70] reported NO decomposition to N₂ and N₂O on reduced Pt/CeO₂ catalysts even at room temperature. Based on previous studies [33–35,70], the transient NO trend in the lean period has the following aspects. First NOx is trapped on sites close to the Pt crystallites. This is followed by slower trapping on distal and sub-surface sites. At the same time NO decomposition occurs on reduced Pt and ceria sites. The nonmonotonic dependence of NOx reduction conversion on O₂ concentration at 150 °C is explained by the simultaneous involvement of two NOx reduction pathways; i.e. the conventional NSR pathway and the redox pathway. As such, for the NSR pathway, NOx is stored on the ceria during the lean feed and the NOx is reduced in the ensuing rich period. Previous studies [4,68] point out that NOx storage typically proceeds through the sequential NO oxidation to NO₂ which then is reactively stored as nitrates. An alternative route involves nitrite formation. A number of studies (e.g. [63]) have shown that Pt catalyzed NO oxidation is of positive order with respect to O₂. Hence, an increase in the O₂ concentration should promote NOx storage on PCA. Thus, for the S_N = 9.7 feed the NSR pathway has a dominant contribution to the NOx conversion as the large excess of O₂ oxidizes the reduced PCA quickly and inhibits NO decomposition on PCA. At the other extreme is the S_N = 0.03 case for which the redox pathway mainly contributes to the NOx conversion as O₂ is excluded in feed. As O₂ is added into the mixture the NO decomposition is inhibited, resulting in a lower NOx conversion. However, compared to the S_N = 9.7 case, the low O₂ concentration in S_N = 0.30 case leads to a lower NO oxidation rate and NOx storage and inferior NOx reduction behavior. This explains the poor NOx abatement performance obtained for the S_N = 0.30 case.

Figs. 6.c, 6.e and 6.g show the transient profiles of N-containing products at 150 °C. With the feed devoid of O₂ (S_N = 0.03), each of the N-containing products (N₂, NH₃ and N₂O) is generated throughout the lean period, confirming the contribution from the redox pathway. The addition of O₂ shortens the generation period. For example, the increase of S_N from 0.03–9.7 shrinks the reduction period to the first 3 s of the lean phase, with larger N₂ (~ 2500 ppm) and N₂O (~ 200 ppm) peaks detected. Recall that O₂ fed during the lean period competes with NO to decompose on vacancies and/or react with residue H₂ on the catalyst, an increase of O₂ concentration in the lean decreases the chance for NO reduction to N₂ and NH₃. Therefore, the generation period of N-containing products shrinks with the addition of O₂. With a large excess of O₂ in feed (S_N = 9.7), the NOx reduction pathway is dominated by the NSR pathway. The generation of N-containing species (N₂, NH₃, N₂O) during the lean period may be attributed to the reaction between the adsorbed reducing species (e.g. NH₃ and H adatoms) and NOx fed [59–61].

Transient profiles of nitrogen-containing species confirm the transition from the redox pathway to the NSR pathway with an increase in the O₂ concentration (S_N). The S_N increase from 0.03 to 9.7 shrinks the duration during which N-containing products (N₂, NH₃ and N₂O) are generated in the rich period and early lean period. Elimination of any N₂, NH₃ and N₂O generation during the late lean phase (i.e., after 15 s in lean phase for the S_N = 9.7 case) shows a transition from some reduction to NOx storage. Correspondingly, the expanded difference between detected NOx and the feed level (300 ppm) is an indicator of NOx storage. Also, with the increase in S_N is the increased formation of

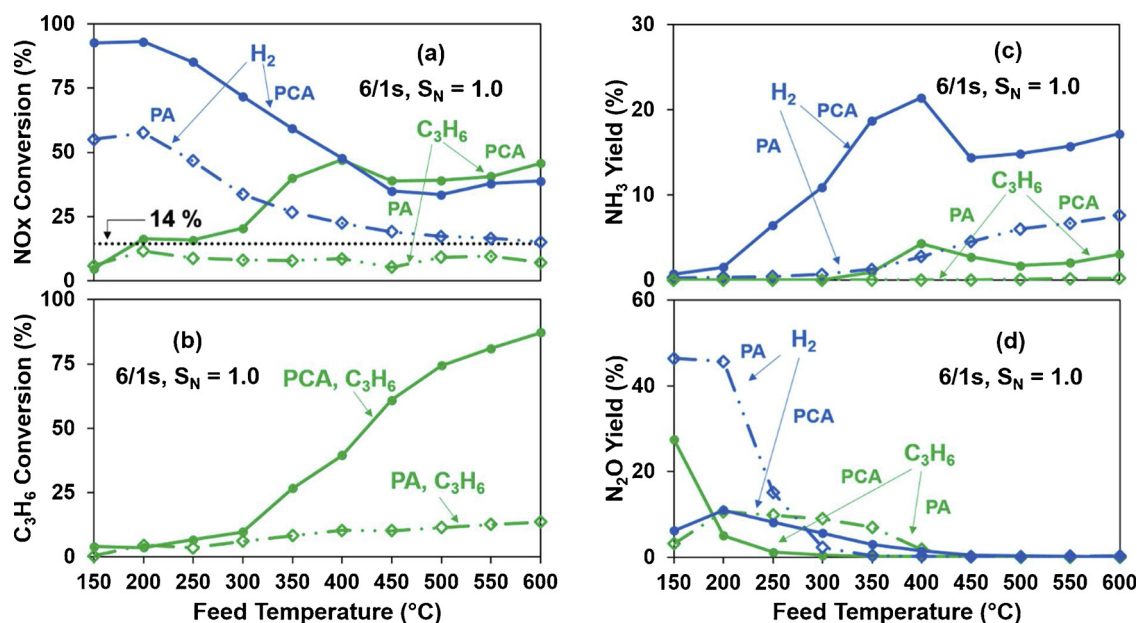


Fig. 7. Cycle-averaged reactant (NOx and C₃H₆) conversions and product (N₂O and NH₃) yields over PCA or PA as a function of feed temperature. [Conditions: lean/rich switching frequency: 6/1 s; lean: 300 ppm NO, 0.5% ppm O₂, balance Ar; rich: 300 ppm NO, 6.21% H₂ or 0.69% C₃H₆, balance Ar].

nitrogen-containing products (N₂, NH₃ and N₂O) during the rich phase.

3.2.2. Impact of reductant

The redox pathway involves NOx reduction on reduced ceria sites, including the ceria sites proximal to PGM particles and isolated ceria sites [25,28]. Previous studies show that the addition of Pt onto ceria leads to two additional active sites in addition to CeO₂ sites; namely, PGM sites and Pt/CeO₂ sites [29,30]. Each of these is able to reduce NO [25,28,29]. Our previous [39] study showed that ceria reduced NO once activated at high temperatures (e.g. > 450 °C). To differentiate the contribution from Pt and Pt/CeO₂ sites and to identify the role of Pt/CeO₂ sites, PCA and PA were compared in targeted experiments described next.

We showed earlier the deNOx performance over PCA and PA for the S_N = 9.7 case and concluded that the NOx storage capacity plays a significant role in NOx conversion. Here we focus on the S_N = 1.0 case; the lower O₂ concentration attenuates the NOx reduction performance contributed by the redox pathway. H₂ and C₃H₆ reductants are used to make our points.

Fig. 7.a shows the cycle-averaged NOx conversion for the S_N = 1.0 cycle over PCA under the fastest cycling (6/1 s). Similar to the S_N = 9.7 case shown earlier (Fig. 4.b), H₂ outperforms C₃H₆ at low and intermediate temperatures (150 °C–400 °C). At high temperature the behavior is different. The NOx conversion approaches 14% for both reductants for the S_N = 9.7 case. In contrast, the NOx conversion is ~35–40% for both reductants for the S_N = 1.0 case. This indicates that some reduction occurs during the lean part of the cycle. Further, C₃H₆ gives a slightly higher NOx conversion than H₂. As discussed earlier, deNOx achieved below 400 °C is a result of NOx storage and reduction. With PCA having a negligible NOx storage capacity but nonzero OSC at higher temperatures, the NOx reduction occurring during the lean feed is a result of the redox pathway. Accordingly, for both the S_N = 9.7 and S_N = 1.0 cases, the inferiority of C₃H₆ to H₂ below 400 °C is a result of differences in their reactivities on Pt. On the other hand, the superiority of C₃H₆ to H₂ above 450 °C for the S_N = 1.0 case is its higher reactivity than H₂ on CeO₂. Wang et al. studied the complete reduction process of CeO₂ [25] and Pt/CeO₂ [26] by H₂ and C₃H₆ and concluded that C₃H₆ leads to a higher extent of reduction on both CeO₂ and Pt/CeO₂. They suggested that it is due to the deposition of carbonaceous species on the ceria surface. The results reported in Fig. 7 corroborate the Wang et al.

findings; i.e. C₃H₆ provides more reducing sites on the CeO₂ (than H₂), either vacancies or carbonaceous material, for subsequent NO decomposition/reduction. Taking this line of reasoning one step further, we showed earlier that the deNOx attributed to the redox pathway is sensitive to the O₂ concentration; i.e., competition between NO and O₂ for reduced sites. The data indicate that a large excess of O₂ in the S_N = 9.7 case results in the fast oxidation of reduced sites by O₂, largely suppressing NO conversion. In the S_N = 1.0 case, the O₂ inhibition is somewhat less with a fraction of NO able to be reduced. As a result, an enhancement of NOx conversion by C₃H₆ exists in the S_N = 1.0 case but not in the S_N = 9.7 case.

To assess the contribution from Pt to that of CeO₂ or even of Pt/CeO₂, the PA sample was evaluated using the same experimental conditions. Fig. 7.a shows the NOx conversion with PA under 6/1 cycling. Similar to the S_N = 9.7 case (Fig. 2.a and .b), PCA is much more active than PA for NOx conversion using either C₃H₆ or H₂ as the reductant. Over the entire temperature range, a higher NOx conversion is achieved with H₂ compared to C₃H₆ for PA. In contrast, our previous study [39] showed that C₃H₆ gave a better deNOx performance than H₂ over CeO₂ under cyclic conditions. These findings suggest that the enhancement of NOx conversion over PCA by C₃H₆ above 450 °C in the S_N = 1.0 case is a result of contribution of the Pt/CeO₂ and/or CeO₂ sites. Fig. 7.b shows the C₃H₆ conversion over PCA and PA samples. The higher C₃H₆ conversion obtained on PCA shows the role of oxygen storage in enhancing oxidation. In the absence of ceria, a large fraction of the O₂ fed during the lean leaves the reactor unreacted.

Fig. 7.c shows the NH₃ yield over PCA and PA with H₂ or C₃H₆ as reductant. For both PCA and PA, H₂ is much more effective in providing H adatoms to react with NO to make NH₃. For PCA the NH₃ yield increases with feed temperature below 400 °C and reaches a plateau above 450 °C (~14% with H₂ and ~3% with C₃H₆). The nonmonotonic dependence of NH₃ yield on feed temperature for PCA may be attributed to the competing temperature dependent NOx and O₂ storage capacities, as we discussed earlier. The NH₃ yield over PA increases monotonically with feed temperature for H₂ feed while remaining at a negligible level for C₃H₆. Finally, Fig. 7.d shows the N₂O yield over PCA and PA. The formation of N₂O is confined to lower temperatures (< 400 °C) with PA giving a slightly higher N₂O yield.

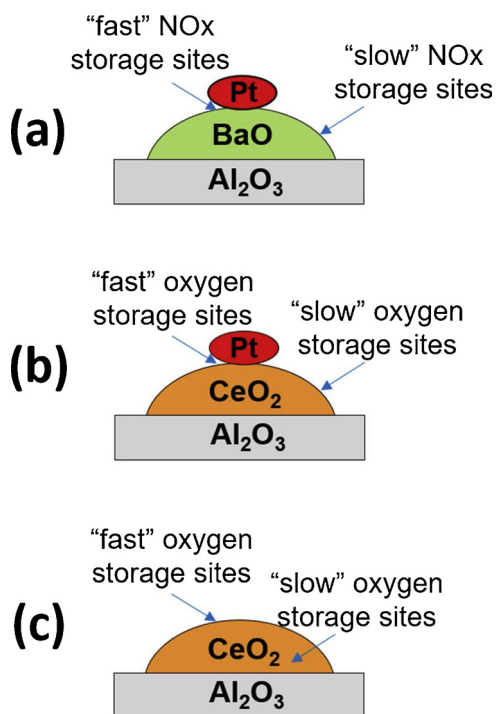


Fig. 8. Fast and slow NO_x or oxygen storage sites. (a) fast and slow NO_x storage sites on PBA; (b) (c) fast and slow oxygen storage sites on PCA. Here BaO and CeO₂ are chosen to represent the NO_x and oxygen storage material respectively.

3.3. Impact of fast cycling

As presented earlier, there are three principal pathways (conventional NSR pathway, HC intermediate pathway, redox pathway) that may contribute to deNO_x performance during lean-rich switching. Earlier the dependence of NO_x conversion and byproduct (NH₃ and N₂O) yield on cycling frequency for PCA catalysts was presented (Fig. 5). The results show that because PCA has NO_x and O₂ storage capacity, both the NSR and redox pathways contribute to extents that depend on the operating conditions. The results for PBA reveal the importance of NO_x storage in enhancing NO_x conversion over a wide range of temperatures (Fig. S4 in Supplementary Material). A comparison of PBA to PCA indicates that the redox pathway may only contribute at high temperature and without an excess of O₂ (Fig. 2). The contribution of the hydrocarbon intermediate pathway is more difficult to assess. Recent findings indicate that it does contribute but its impact is secondary. In this section we focus on the impact of cycle frequency on the deNO_x performance and explain the impact in the context of the two pathways.

It is instructive to compare and contrast the storage and utilization of NO_x and O₂. Fig. 8 shows schematics of the locale of an individual Pt and/or CeO₂ particle for the PBA and PCA catalysts. Fig. 8.a depicts the fast and slow NO_x storage sites on the Pt/BaO (or Pt/CeO₂ at low temperature). Previous works have described how the local structure of the NSR catalyst defines at least two populations of sites; specifically proximal and distal NO_x storage sites [23,44]. Kumar et al. [65] showed experimentally that the storage and regeneration of NO_x during NSR involves an active interface at the contact line of the PGM crystallite and NO_x storage material. These measurements provided an experimental underpinning of a coupled process of catalytic reaction and transport. Under conditions that the NO supply is limiting, the diffusion of stored or adsorbed NO_x species to and from storage sites is the rate controlling process. The process was modeled at the crystallite scale by Bhatia et al. [66] and Shakya et al. [67]. A simplified picture (and model) comprises “fast” and “slow” NO_x storage sites, the former of which are proximal site and the latter distal. The primary pathway

for NO_x storage involves sequential steps. First, NO and O₂ adsorb and react on the Pt, forming NO₂. The NO₂ then moves to a storage sites via the gas phase which involves desorption and gas phase transport, or via the surface, which involves spillover and surface or solid-state diffusion.

Fig. 8.b is a schematic picture of the Pt/CeO₂ catalyst which, instead of storing and consuming NO_x, stores and consumes O₂. The PCA catalyst comprises fast and slow oxygen storage sites based on the analogous premise of proximity of the CeO₂ to the PGM crystallite [29]. Fast oxygen storage sites are defined as the proximal to Pt particles whereas slow oxygen storage sites are defined as storage sites far away from Pt particles. A second pair of fast and slow oxygen storage sites can be designated according to the position on/within a CeO₂ particle, as per Fig. 8.c, following our previous study on NO decomposition over PGM-free ceria. The reduction of PGM-free ceria first undergoes a fast surface reduction process and then continues with slow consumption of oxygen diffusing from the bulk to the surface. As the surface oxygen is more accessible than bulk oxygen, the “fast” oxygen storage sites are the oxygen sites on the surface of ceria particles while the “slow” oxygen storage sites are the oxygen sites inside ceria particles.

For both the NSR and redox pathways, enhancement in the NO_x conversion by rapid pulsing with a reductant can be ascribed as the more efficient utilization of fast sites, be they NO_x storage sites or oxygen storage sites. During cyclic NSR process, the occupation and regeneration starts with the utilization of fast NO_x storage sites and then proceeds with slow NO_x storage sites. As pointed out in previous studies [23,43], faster switching between lean and rich feeds through a shorter cycle results in less loss of NO_x. That is, a longer lean period ultimately results in the breakthrough of NO/NO₂ as the diffusion to sites further removed from the PGM crystallite is too slow compared to the characteristic residence time of the flowing gas. As fast NO_x storage sites offers easier accessibility and faster occupation/regeneration rates, fast cycling leads to a higher NO_x conversion in the NSR pathway.

A similar picture is envisioned for the redox pathway. This involves the generation of reducing components (vacancies and accumulating surface intermediates) during the rich phase feed with the subsequent adsorption and decomposition/reduction of NO_x during the lean feed. Faster switching between lean and rich streams enable a more efficient utilization of the oxygen storage sites. During cyclic experiments, the occupation and regeneration first starts with the utilization of fast oxygen storage sites and then proceeds with slow oxygen storage sites. As fast oxygen storage sites offer easier accessibility and faster occupation/regeneration rates, fast cycling leads to a higher NO_x conversion via the redox pathway.

When C₃H₆ is the reductant, the working mechanisms are more complex due to the potential involvement of surface hydrocarbon intermediate species. Compared to H₂, the injection of C₃H₆ onto both PBA and PCA results in a reduced PGM surface with accumulation of hydrocarbon species [16,26]. The adsorbed species may be further utilized for NO_x reduction, either through interaction with adsorbed NO_x for intermediates R-NO_x and finally N₂ in NSR pathway [14,16], or through interaction with NO and/or O₂ for additional NO reduction in redox pathway. At high temperatures (> 550 °C), the utilization of C₃H₆ results in a deeper reduction extent of ceria with accumulation of hydrocarbon intermediates [25,26]. These intermediates on serve as additional reductant and enhance NO reduction via the redox pathway.

The promotion of C₃H₆ shows better resistance to O₂ during NSR. Enhancement of NO_x conversion by C₃H₆ via a redox pathway decreases monotonically with increased O₂ concentration in the feed, or increased S_N (Fig. S5 in Supplementary Material [64]), eventually becoming negligible in a large excess of O₂ (e.g. S_N = 9.7, Fig. 4b, > 450 °C). In contrast, the enhancement of NO_x conversion by C₃H₆ during the NSR pathway is sustained in the S_N = 9.7 case (Fig. 4a). The better resistance in the NSR pathway may be ascribed to the incorporation of stored NO_x on storage sites (e.g. BaO). In the redox pathway, the hydrocarbon intermediates formed on PGM sites are

rapidly consumed by NO and O₂ with O₂ exhibiting a better oxidation capability on reduced surface. With a large excess of O₂ in the feed, hydrocarbon intermediates accumulating on the PCA will be first scavenged by O₂, diminishing the likelihood of NO reduction. In contrast, over NSR catalyst (e.g. PBA), any accumulated hydrocarbon intermediates PGM are able to react directly with stored NOx, which enables enhanced NOx conversion by C₃H₆ at high temperatures in a lean atmosphere.

4. Conclusions

Experiments of NOx reduction under fast lean/rich cycling over Pt/Al₂O₃, Pt/CeO₂/Al₂O₃ and Pt/BaO/Al₂O₃ provide insight into the underlying mechanism and elucidate the beneficial impacts from storage components (i.e. BaO and CeO₂). The impacts of catalyst formulation, reductant type, O₂ concentration, and cycling time were evaluated.

With cycle-averaged lean feeds (S_N = 9.7) and H₂ as reductant, Pt/CeO₂/Al₂O₃ (PCA) exhibits the highest NOx conversion below 300 °C while Pt/BaO/Al₂O₃ (PBA) surpasses PCA above 300 °C. Above 450 °C, NOx reduction over PCA is largely confined to only the rich feed but PCA still surpasses Pt/Al₂O₃ (PA) for a small enhancement in the NOx conversion. Generally, the overall NOx conversion over the three catalysts parallels the corresponding NOx storage capacity. The dependence of NOx conversion on NOx storage capacity underscores the necessity of NOx storage functionality under lean conditions. In contrast, the oxygen storage functionality only shows rather confined promotion. Pathways involved in adsorbed NOx, including the conventional NSR pathway and the hydrocarbon intermediate pathway, are responsible for the effective NOx reduction during fast cycling. The redox mechanism plays a rather minor role.

NO reduction over PCA by H₂ can be achieved in both lean and rich with anaerobic feeds within the whole temperature range (150 °C ~ 600 °C). With the addition of excess O₂ NOx conversion over PCA increases below 400 °C but decreases above 400 °C. The opposing trends can be attributed to the dependence of NOx storage and/or oxygen storage capacity of PCA on temperatures. PCA mainly exhibits NOx storage capacity at lower temperatures (i.e. < 400 °C) and the enhancement from excess O₂ comes from the increased NOx storage rates. At higher temperatures (i.e. > 400 °C), PCA only exhibits oxygen storage capacity. The detrimental impact from excess O₂ results from competition between NO and O₂ for reduced sites (vacancies and adsorbed reducing intermediates).

Fast cycling enhances NOx conversion over PBA in the lean case and over PCA for the stoichiometric case within the whole temperature range using H₂ as the reductant. The promotional impact over PCA for the lean case only exists at low temperatures (< 450 °C), when PCA maintains NOx storage capacity. The promotional impact from fast cycling can be ascribed to the better utilization of fast NOx or oxygen storage sites from the conventional NSR pathway or redox pathway correspondingly. With a cycle-averaged rich and stoichiometric feed, lean/rich cyclic operation is inferior to steady state operation. However, lean/rich cyclic operation surpasses steady state operation with the presence of slightly excess O₂.

Enhanced NOx conversion was also observed by adopting fast cycling and/or C₃H₆ as reductant over PBA in the lean case or over PCA in the stoichiometric case. Compared to H₂, reduction of PBA and PCA by C₃H₆ results in surface-deposited hydrocarbon fragments on Pt and/or ceria, which can be further utilized by stored NOx on PBA or gaseous fed NO in rich. The additional reduction extent of PBA and PCA provided by C₃H₆ may account for the enhancement of overall NOx conversion by C₃H₆. The enhancement from C₃H₆ is more resistant to O₂ in NSR pathway than the redox pathway. The presence of H₂O and CO₂ inhibits the enhancement by C₃H₆ in both PBA and PCA cases mainly due to the competition for NOx or oxygen storage sites.

This study confirms the prevalence of the conventional NSR mechanism and the hydrocarbon intermediate pathways during fast

cycling over NSR catalysts. A redox pathway is validated but proven to extend a rather limited impact on NOx abatement under excess O₂. Fast cycling exhibits enhancement over PBA in S_N = 9.7 case and over PCA in S_N = 1.0 case, thanks to the improved utilization of fast NOx storage and oxygen storage (or vacancy) sites respectively. C₃H₆ leads to an enhanced NOx conversion over PBA in the S_N = 9.7 case and over PCA in the S_N = 1.0 case. The benefits from C₃H₆ may be ascribed to the deposition of hydrocarbon fragments on Pt sites, which serve as additional reduction of stored NOx or gaseous NO in NSR or redox pathway respectively.

Acknowledgement

This work was supported by the University of Houston and DOE-EERE (DE-EE0008233).

Appendix A. Supplementary data

Supplementary material related to this article can be found, in the online version, at doi:<https://doi.org/10.1016/j.apcatb.2019.05.044>.

References

- [1] T. Johnson, SAE Int. J. Engines 6 (2014) 699–715.
- [2] N. Takahashi, H. Shinjoh, T. Iijima, T. Suzuki, K. Yamazaki, K. Yokota, H. Suzuki, N. Miyoshi, K. Matsumoto, T. Tanizawa, T. Tanaka, S. Tateishi, K. Kasahara, Catal. Today 27 (1996) 63–69.
- [3] S. Brandenberger, O. Krocher, A. Tisser, R. Althoff, Catal. Rev. 50 (2008) 492–531.
- [4] W.S. Epling, L.E. Campbell, A. Yezzerets, N.W. Currier, J.E. Parks II, Catal. Rev. 46 (2004) 163–245.
- [5] M.P. Harold, Curr. Opin. Chem. Eng. 1 (2012) 303–301.
- [6] K. Kamasamudram, N.W. Currier, X. Chen, A. Yezzerets, Catal. Today 151 (2010) 212–222.
- [7] Y. Liu, Y. Zheng, M.P. Harold, D. Luss, Appl. Catal. B 132–133 (2–13) (2019) 293–303.
- [8] P. Forzatti, L. Liotti, I. Nova, E. Tronconi, Catal. Today 151 (2010) 202–211.
- [9] N. Waldbuesser, J. Guenther, H. Hoffmann, O. Erlenmayer, F. Duvinage, C. Enderle, J. Schommers, D. Waeller, SAE Tech Paper (2010) 2010-01-1172.
- [10] K.J. Lee, P.A. Kumar, M.S. Maqbool, K.N. Rao, W.H. Song, H.P. Ha, Appl. Catal. B 142–143 (2013) 705–717.
- [11] H.-Y. Chen, S. Mulla, E. Weigert, K. Camm, T. Ballinger, J. Cox, P. Blakeman, SAE Int. J. Fuels Lubr. 6 (2013) 372–381.
- [12] M. Naseri, C. Aydin, S. Mulla, R. Conway, S. Chatterjee, SAE Int. J. Engines 8 (2015) 1144–1151.
- [13] P.S. Dhillion, M.P. Harold, D. Wang, A. Kumar, S.Y. Joshi, Chem. Eng. J. (2018) in press.
- [14] Y. Bisaiji, K. Yoshida, M. Inoue, K. Umamoto, T. Fukuma, SAE Int. J. Fuels Lubr. 5 (2012) 380–388.
- [15] L. Liotti, L. Castoldi (Eds.), NOx Trap Catalysts and Technologies: Fundamentals and Industrial Applications, Royal Society of Chemistry, 2018.
- [16] M. Inoue, Y. Bisaiji, K. Yoshida, N. Takagi, T. Fukuma, Top. Catal. 56 (2013) 3–6.
- [17] C.C.Y. Perng, V.G. Easterling, M.P. Harold, Catal. Today 231 (2014) 125–134.
- [18] A. Reihani, B. Patterson, J. Hoard, G.B. Fisher, J.R. Theis, C.K. Lambert, J. Eng. Gas Turbines Power 139 (2017) 102805.
- [19] M. Li, Y. Zheng, M.P. Harold, D. Luss, Emission Control Science and Technology, (2017), pp. 1–15.
- [20] A.W.-L. Ting, M.P. Harold, V. Balakotaiah, Chem. Eng. Sci. 189 (2018) 413–421.
- [21] Y. Bisaiji, K. Yoshida, M. Inoue, N. Takagi, T. Fukuma, SAE Int. J. Fuels Lubr. 5 (2012) 1310–1316.
- [22] A. Reihani, B. Corson, J.W. Hoard, G.B. Fisher, E. Smirnov, D. Roemer, J. Theis, C. Lambert, SAE Int. J. Engines 9 (2016) 1630–1641.
- [23] A.W.-L. Ting, M. Li, M.P. Harold, V. Balakotaiah, Chem. Eng. J. 9 (2017) 2935–2938.
- [24] A.W.-L. Ting, M.P. Harold, V. Balakotaiah, Catal. Lett. 148 (2018) 1951–1964.
- [25] Y. Wang, J.P. de Boer, F. Kapteijn, M. Makkee, Chem. Cat. Chem. 8 (2016) 102–105.
- [26] Y. Wang, F. Kapteijn, M. Makkee, Appl. Catal. B 231 (2018) 200–212.
- [27] Y. Wang, M. Makkee, Appl. Catal. B 223 (2018) 125–133.
- [28] Y. Wang, R. Oord, D. van den Berg, B.M. Weckhuysen, M. Makkee, Chem. Cat. Chem. 9 (2017) 2935–2938.
- [29] A. Trovarelli (Ed.), Catalysis by Ceria and Related Materials, Imperial College Press, London, 2002.
- [30] A. Trovarelli, Catal. Rev. 38 (1996) 439–520.
- [31] W. Lang, P. Laing, Y. Cheng, C. Hubbard, M.P. Harold, Appl. Catal. B 218 (2017) 430–442.
- [32] A. Bueno-Lopez, Appl. Catal. B 146 (2014) 1–11.
- [33] Y. Ren, M.P. Harold, ACS Catal. 1 (2011) 969–988.
- [34] C. Shi, Y. Ji, U.M. Graham, G. Jacobs, M. Crocker, Z. Zhang, Y. Wang, T.J. Toops, Appl. Catal. B 119–120 (2012) 183–196.
- [35] Y. Ji, T.J. Toops, U.M. Graham, G. Jacobs, M. Crocker, Catal. Lett. 110 (2006)

- 29–27.
- [36] Y. Ryou, J. Lee, H. Lee, C.H. Kim, D.H. Kim, *Catal. Today* 307 (2018) 93–101.
- [37] A. Filtschew, C. Hess, *Appl. Catal. B* 237 (2018) 1066–1081.
- [38] Y. Wang, M. Makkee, *Appl. Catal. B* 221 (2018) 196–205.
- [39] Z. Zhou, M.P. Harold, D. Luss, *Appl. Catal. B* 240 (2019) 79–91.
- [40] Y. Zheng, M. Li, M.P. Harold, D. Luss, *SAE Int. J. Engines* 8 (2015) 1117–1125.
- [41] Y. Zheng, M. Li, M.P. Harold, D. Luss, *Catal. Today* 267 (2016) 192–201.
- [42] K. Uenishi, K. Umamoto, T. Yoshida, T. Itoh, Fukuma, *Int. J. Auto. Tech-Kor* 5 (2014) 115–120.
- [43] A. Reihani, G.B. Fisher, J.W. Hoard, J.R. Theis, J.D. Pakko, C.K. Lambert, *Appl. Catal. B* 223 (2018) 177–191.
- [44] W.S. Epling, J.E. Parks, G.C. Campbell, A. Yezerets, N.W. Currier, L.E. Campbell, *Catal. Today* 96 (2004) 21–30.
- [45] B. Westerberg, E.J. Fridell, *J. Mol. Catal. A Chem.* 165 (2001) 249.
- [46] D. Uy, A. O'Neil, W. Weber, *Appl. Catal. B* 35 (2002) 219.
- [47] Y. Li, S. Roth, J. Dettling, T. Buetel, *Top. Catal.* 16–17 (2001) 139.
- [48] H. Abdulhamid, E. Fridell, M. Skoglundh, *Top. Catal.* 30–31 (2004) 161.
- [49] M. Al-Harbi, D. Radtke, W.S. Epling, *Appl. Catal. B* 96 (2010) 524–532.
- [50] V. Easterling, Y. Ji, M. Crocker, M. Dearth, R.W. McCabe, *Appl. Catal. B* 123–124 (2012) 339–350.
- [51] R.D. Clayton, M.P. Harold, V. Balakotaiah, *Appl. Catal. B* 84 (2008) 616–630.
- [52] J.A. Pihl, J.E. Parks II, C.S. Daw, T.W. Root, *SAE Technical Paper* (2006) 2006-01-344.
- [53] A. Kumar, M.P. Harold, V. Balakotaiah, *J. Catal.* 270 (2010) 214–223.
- [54] S. Bartova, P. Koci, D. Mracek, M. Marek, J.A. Pihl, J.-S. Choi, T.J. Toops, W.P. Partridge, *Catal. Today* 231 (2014) 145–154.
- [55] A. Martinez-Arias, J. Soria, J.C. Conesa, X.L. Seoane, A. Arcoya, R. Cataluna, J. Chem. Soc. Faraday Trans. 91 (1995) 1679–1687.
- [56] L. Lietti, I. Nova, P. Forzatti, *J. Catal.* 257 (2008) 270–282.
- [57] G. Jacobs, L. Williams, U. Graham, D. Sparks, B.H. Davis, *J. Phys. Chem. B* 107 (2003) 10398–10404.
- [58] <https://webbook.nist.gov/cgi/cbook.cgi?ID=C10024972&Mask=200#Mass-Spec>.
- [59] J.P. Breen, R. Burch, C. Fontaine-Gautrelet, C. Hardacre, C. Rioche, *Appl. Catal. B* 81 (2008) 150–159.
- [60] S. Chansai, R. Burch, C. Hardacre, S. Naito, *J. Catal.* 317 (2014) 91–98.
- [61] P. Dasari, R. Muncief, M.P. Harold, *Top. Catal.* 56 (2013) 1922–1936.
- [62] C. Binet, M. Daturi, J.-C. Lavalley, *Catal. Today* 50 (1999) 207–225.
- [63] M. Crocoll, S. Kureti, W. Weisweiler, *J. Catal.* 229 (2005) 480–489.
- [64] S.A. Malamis, M. Li, W.S. Epling, M.P. Harold, *Appl. Catal. B* 237 (2018) 588–602.
- [65] A. Kumar, M.P. Harold, M.P. Harold, V. Balakotaiah, *J. Catal.* 270 (2010) 214–223.
- [66] D. Bhatia, R.D. Clayton, M.P. Harold, V. Balakotaiah, *Catal. Today* 147 (2009) 250–256.
- [67] B.M. Shakyia, M.P. Harold, V. Balakotaiah, *Catal. Today* 184 (2012) 27–42.
- [68] S. Roy, A. Baiker, *Chem. Rev.* 109 (2009) 4054–4091.
- [69] S.S. Chaugule, A. Yezerets, N.W. Currier, F.H. Ribeiro, W.N. Delgass, *Catal. Today* 151 (2010) 291–303.
- [70] M. Haneda, Y. Kintaichi, H. Hamada, *Phys. Chem. Chem. Phys.* 4 (2002) 3146–3151.
- [71] A.W.-L. Ting, V. Balakotaiah, M.P. Harold, *Chem. Eng. J.* 370 (2019) 1493–1510.
- [72] T.J. Toops, D.B. Smith, W.S. Epling, J.E. Parks, *Appl. Catal. B* 58 (2005) 255–264.
- [73] R.D. Clayton, M.P. Harold, V. Balakotaiah, *AIChE J.* 55 (2009) 687–700.
- [74] M. Makkee, Y. Wang, *SAE Int. J. Engines* 10 (2017) 1573–1579.
- [75] Y. Wang, J.P. de Boer, F. Kapteijn, M. Makkee, *Top. Cat.* 59 (2016) 854–860.